Nuclear Factor-κB Affects Tumor Progression in a Mouse Model of Malignant Pleural Effusion

Georgios T. Stathopoulos, Zhiwen Zhu, M. Brett Everhart, Ioannis Kalomenidis, William E. Lawson, Semra Bilaceroglu, Todd E. Peterson, Daphne Mitchell, Fiona E. Yull, Richard W. Light, and Timothy S. Blackwell

Department of Medicine, Division of Allergy, Pulmonary and Critical Care Medicine, Department of Cell and Developmental Biology, and Department of Cancer Biology, Vanderbilt University School of Medicine; Department of Veterans Affairs, VA Tennessee Valley Healthcare System; Department of Radiology and Radiological Sciences, Vanderbilt Institute of Imaging Science; Pulmonary Division, Saint Thomas Hospital, Nashville, Tennessee; Department of Pulmonary Medicine, 1st affiliated Hospital of Zhongshan (Sun Yat-sen) University, Guangzhou, Guangdong, China; and Department of Critical Care and Pulmonary Services, Evangelismos Hospital, School of Medicine, University of Athens, Greece

We developed a novel mouse model of malignant pleural effusion (MPE) by injecting Lewis lung cancer (LLC) cells directly into the pleural space of syngeneic C57B/6 mice. The pleural effusions in this model share common cellular and biochemical features with human MPEs. Implantation and growth of pleural tumors triggers a host inflammatory response characterized by a mixed inflammatory cell influx into the pleural fluid. LLC cells exhibited high basal nuclear factor (NF)-κB activity *in vitro* and *in vivo*, which we used to drive expression of a NF-κB–dependent green fluorescent protein-firefly luciferase fusion reporter construct. NF-κB–dependent reporter expression allowed intravital tracing of pleural tumors. Inhibition of NF-κB in LLC cells did not affect cell viability in culture; however, injection of LLC cells expressing a dominant NF-κB inhibitor resulted in decreased tumor burden, decreased pleural effusion volume, and decreased pleural effusion TNF-α levels. These studies indicate that tumor NF-κB activity regulates pleural tumor progression. This reproducible model of MPE can be used to further study the influence of specific host and tumor factors on the pathogenesis of MPE and evaluate new therapeutic strategies.

Keywords: Lewis lung cancer; lung; adenocarcinoma; bioluminescence; luciferase

Malignancy involving the pleura is the third leading cause of pleural effusions, with an annual incidence of $> 150{,}000$ cases in the United States (1, 2). Adenocarcinomas account for $\sim 70\%$ of all malignant pleural effusions (MPEs), with lung adenocarcinomas being the most frequent underlying malignancy (3). The appearance of a MPE is an ominous prognostic sign for patients with cancer, because the presence of the MPE indicates that the tumor is incurable by surgery and life expectancy is short (1). In addition, the presence of the pleural effusion can cause dyspnea that severely compromises the quality of the patient's life (4, 5). Pleurodesis, the iatrogenic induction of pleural fibrosis to obliterate the pleural cavity, is commonly used to prevent symptomatic re-accumulation of pleural effusions; however, this therapy is often ineffective and is associated with significant morbidity (6). Therefore, there is a need to develop novel treatment methods based on a better understanding of the pathobiology of pleural fluid accumulation.

It is generally believed that disruption of the endothelial–mesothelial barrier, increased capillary permeability, tumor-induced angiogenesis, and lymphatic obstruction are responsible for the exudation of increased amounts of fluid into the pleural cavity (1, 7). However, the specific mechanisms underlying pleural fluid accumulation are poorly defined because studies of MPE pathogenesis are limited by a lack of animal models that reproduce the pathobiology of human MPE. Although mouse models that require immunocompromised mice for propagation of human cancer cells mice have provided insights into the biological behavior of tumor cells in the pleural cavity (7–9), these models are not ideal because the host is immunocompromised, and, therefore, the host immune response is attenuated or missing. The immune response against tumor may be an important component in the development of MPE because host inflammatory cells may contribute to or regulate the production of mediators that affect pathogenesis (10).

Nuclear factor (NF)-κB is a ubiquitous family of transcription regulatory proteins that affects a variety of cellular functions and influences tumor biology and host–tumor interactions. NF-κB is activated by a number of tumor-promoting agents and is involved in the production of proteins that enhance cell survival and proliferation (11). High basal NF-κB activation is present in lung adenocarcinoma cells and human lung cancer, and inhibition of NF-κB sensitizes tumor cells to apoptosis and the effects of chemotherapeutic agents (11–15).

Lewis lung cancer (LLC) cells are derived from a spontaneously arising lung adenocarcinoma in C57B/6 mice. These cells are characterized by short doubling times *in vitro* and *in vivo* and aggressive biological behavior. They can be propagated in wild-type C57B/6 mice, giving rise to lung adenocarcinomas (16–18). In these studies, we have developed and characterized a new murine model of MPE after instillation of lung adenocarcinoma cells in the pleural space of immunocompetent mice. We used this model to investigate whether the NF-κB pathway in tumor cells is linked to MPE formation and progression of pleural carcinomatosis.

MATERIALS AND METHODS

Cell Line, Culture, and Transfection

LLC cells were purchased from the American Type Culture Collection (Manassas, VA) and were cultured at 37°C in 5% CO_2-95% air using Dulbecco's modified Eagle's medium 10% FCS supplemented with glutamine and 100 mg/liter penicillin/streptomycin.

A NF-κB reporter plasmid (NF-κB–enhanced green fluorescent protein-luciferase plasmid [pNGL]) was used for LLC cell transfection.

(*Received in original form April 10, 2005 and in final form September 11, 2005*)

This work was supported by NIH HL66196, NIH HL61419, and the Department of Veterans Affairs. G.T.S. was supported by a scholarship by the Greek State Scholarship Foundation (IKY). T.E.P. was supported by a Career Award at the Scientific Interface from the Burroughs Wellcome Fund.

Correspondence and requests for reprints should be addressed to Georgios T. Stathopoulos, M.D., Division of Allergy, Pulmonary and Critical Care Medicine, Vanderbilt University School of Medicine, T-1218 MCN, Nashville, TN 37232-2650. E-mail: georgios.stathopoulos@vanderbilt.edu

Am J Respir Cell Mol Biol Vol 34. pp 142–150, 2006
Originally Published in Press as DOI: 10.1165/rcmb.2005-0130OC on October 6, 2005
Internet address: www.atsjournals.org

pNGL contains eight decameric NF-κB binding sites (GGGACTTTCC) and a minimal herpesvirus thymidine kinase promoter driving expression of an enhanced green fluorescent protein (GFP)-luciferase fusion reporter gene and a neomycin resistance cassette. After transfection of LLC cells with pNGL using Superfect (Qiagen, Valencia, CA), stably expressing clones were selected by addition of G418 (Mediatech, Herndon, VA) at a concentration of 800 μg/ml medium for 10 d. The resulting cell population was screened for reporter expression by fluorescent microscopy, and multiple GFP-expressing colonies were selected, isolated, pooled, and subcultured using G418 at a concentration of 400 μg/ml medium.

For intrapleural injections, pNGL LLC cells were harvested from culture dishes during log-phase growth using a 2-min exposure to a solution of 0.25% trypsin-0.02% EDTA, washed with Ca^{2+}- and Mg^{2+}-free Hanks' balanced salt solution, resuspended in PBS, and titrated using a hemocytometer. Cell viability was assessed using the cellular Trypan blue exclusion test before intrapleural injection. Only cell populations with > 90% viable cells were used for experiments.

Animal Model

C57B/6 mice were purchased from The Jackson Laboratory (Bar Harbor, ME) and inbred in the Vanderbilt University Medical Center Animal Care facility. All animal care and experimental procedures were approved by and conducted according to Institutional Animal Care and Use guidelines. Mice used for experiments were sex-, weight (20–25 g)-, and age (8–12 wk)-matched.

For intrapleural injection, mice were anesthetized by isoflurane anesthesia administered by a VetEquip V-10 anesthesia machine (VetEquip Inc., Pleasanton, CA). The skin overlying the anterior and lateral chest wall was shaved and disinfected, and a 5-mm-long transverse skin incision was made on the left anterolateral thoracic area at the xiphoid level. Fascia and muscle were retracted, and 1.5×10^5 LLC cells suspended in 50 μl PBS were injected into the pleural cavity through an intercostal space under direct observation. The skin incision was closed using continuous 5-0 Ethilon monofilament suture, and the animals were observed until complete recovery. The procedure was not associated with mortality or morbidity.

After 14 d, mice were killed by CO_2 asphyxiation (n = 50), and blood was drawn from the retro-orbital veins (two additional animals were killed at Days 8, 10, and 12). Thereafter, the abdominal wall was cut down, and the viscera were retracted to visualize the diaphragm. Pleural fluid was gently aspirated using a 3-ml syringe, and its volume was measured with a 1000-μl pipette. For histology, lungs were inflated with 10% neutral buffered formalin (volume = 1 ml), explanted, and fixed in the same solution. Samples of the hemidiaphragms and the chest wall were also fixed in formalin for histology. To obtain normal pleural fluid from mice (n = 5), a 30-μl gel-loading pipette tip was inserted through an intercostal space to the posterior paraspinal sulcus immediately after the animals were killed, and pleural fluid was gradually aspirated.

Computed Tomography and Positron Emission Tomography Scanning

Computed tomography (CT) images were acquired on an ImTek micro-CAT II scanner (ImTek Inc., Knoxville, TN) using a tube voltage of 80 kVp and current of 500 μA. A total of 360 projections were acquired over 360 degrees (600 msec exposure per projection), and the images were reconstructed on a 512^3 grid with 125 μm isotropic voxel size. The positron emission tomography (PET) images were acquired using a microPET Focus scanner (Concorde Microsystems, Knoxville, TN). Twenty-minute PET scans were begun between 60 and 70 min after retro-orbital injection of 200–300 μCi of 18-fluoro-6-deoxy-glucose (FDG). Reconstructed PET images had pixel dimensions of $(0.47\ mm)^2$ and 0.82-mm slice thickness. The PET images were acquired immediately after the CT using a common animal holder and with the mouse under anesthesia as described previously for the duration of the imaging session. The animal holder possessed four fiducial markers visible in CT and PET, which facilitated co-registration of the images using the AMIDE software package (The Free Software Foundation Inc., Boston, MA).

Surface Pleural Tumor Enumeration

Because pleural tumors were evenly distributed between visceral and parietal pleural surfaces, only visceral implantations were enumerated, excluding primary tumors at the injection site that occurred occasionally. Tumor implantations on the visceral pleura were counted by two independent readers under a dissecting microscope, and the average number was used for data analyses.

Histology

Mouse lungs, chest walls, and diaphragms were fixed in 10% neutrally buffered formalin for 24 h and 70% ethanol for 3 d. Tissues were embedded in paraffin, and 5-μm-thick sections were cut, mounted on glass slides, and stained with hematoxylin-eosin. Alternatively, slides were coverslipped using low-fluorescence mounting medium and studied under fluorescent microscopy.

Biochemical Assays

Pleural fluid and serum glucose levels were measured using a FreeStyle blood glucose monitor (TheraSense Inc., Alameda, CA). Protein content was determined using the bicinchonic acid protein assay method (Pierce, Rockford, IL). Lactate dehydrogenase (LDH) was measured in 2- to 10-fold diluted pleural fluid and serum using the ADVIA-1650 (Bayer Diagnostics, Leverkusen, Germany) (range 120–220), and results were back-calculated to original volumes.

Cytology

Fifty thousand pleural fluid cells were used for cytocentrifugal specimen (cytospin) preparation. The slides were air dried, fixed in methanol for 10 s, and stained with modified Wright's Giemsa stain or counterstained with 4,6-diamidino-2-phenylindole and mounted in low-fluorescence mounting medium. Distinct cell types were enumerated as a percentage of cells on the slide (200 cells per slide were counted). The cytospins were also examined using fluorescent microscopy to discriminate cancer cells based on GFP expression.

Pleural Permeability Assay

Mice bearing MPEs (n = 8, Day 13) and untreated mice (n = 4) received 200 μl of 50 mg/ml Evans' blue solution (total dose 10 mg) intravenously and were killed 1 h later. Pleural fluid and serum Evans' blue concentration were determined by measuring absorbance at a wavelength of 630 nm in comparison to standards of known Evans' blue concentrations.

ELISA

Serum and pleural fluid samples were assayed for TNF-α, vascular endothelial growth factor (VEGF), monocyte chemoattractant protein (MCP)-1, and MCP-5 using commercially available mouse ELISA kits (R&D Systems, Minneapolis, MN) according to the manufacturer's instructions (detection limits: 3.0, 5.1, 2.0, and 7.0 pg/ml, respectively).

Flow Cytometry

After hypotonic red blood cell lysis, pleural fluid cells were suspended in PBS 3% BSA, stained with phycoerythrin-Cy7-conjugated anti-CD11b antibody (Becton-Dickinson Pharmingen, Palo Alto, CA) at 0.1 μg/10^6 cells for 30 min, and were analyzed by flow cytometry for GFP and CD11b expression using a FACS-SCAN automated flow cytometer (Becton-Dickinson, Palo Alto, CA). Flow cytometric data were analyzed using the WinMDI 2.8 software (J. Trotter, The Scripps Research Institute, La Jolla, CA).

Bioluminescence Imaging

For *in vivo* bioluminescence imaging, mice were anesthetized with isoflurane. The anterior chest wall was shaved, and 100 μl of 10 mg/ml solution of D-luciferin (Biosynth AG, Naperville, IL) (1 mg total dose) was administered by retro-orbital injection. Mice were placed in a light-tight box under continuous anesthesia and imaged as previously described (19–21). Bioluminescence imaging was performed 2 h and 4, 7, 11, and 14 d after pNGL LLC cell injection using the Xenogen IVIS cooled charged coupled device (Xenogen Corporation, Alameda, CA). Data were collected and analyzed using the Living Image v.2.50

(Xenogen) and IgorPro (Wavemetrics, lake Oswego, OR) image analysis software. A photographic image of the animals was first acquired. Subsequently, a bioluminescence image was acquired by integration of photon flux over each group of pixels (bin) in the field of view and graphically represented using an arbitrary pseudo-color scale ranging from 2×10^4 to 10^5 photons/s. A 15-s acquisition time was selected to avoid saturating the camera, and the same imaging parameters (instrument defaults) and pseudo-color scale range were used throughout the experiments. Standard-sized circular regions of interest encompassing the murine chest were determined, and photon flux was measured over these areas.

For bioluminescence imaging of live cells in culture, standard 12-well plates were used. D-luciferin was added to the medium to a final concentration of 0.1 mM, and cells were imaged using the procedure described previously. Image analysis was performed as for *in vivo* imaging, but region of interest sizes matching the culture well area were used.

Adenoviral Vectors and Transient LLC Cell Infection

The replication-deficient recombinant adenoviral vector (Ad) type 5 was used. The adenoviral vector expressing a dominant negative inhibitor of NF-κB (IκBα-DN), which represents a S36–40A mutant of the avian IκB-α that cannot be phosphorylated or degraded, has been previously reported (21). IκBα-DN is denominated "dominant negative" with respect to native IκBα because it binds and sequesters cytoplasmic NF-κB dimers in a nonreversible fashion. Adenoviral vectors expressing β-galactosidase (βgal) and GFP were a gift from Dr. A. Powers (Vanderbilt University, Nashville, TN). Adenoviral vectors were propagated, purified, and stored at −70°C. LLC cells were infected *in vitro* at moi = 500 for 24 h (these conditions gave optimal results during viral titration studies) and subsequently used for experiments.

Cellular Assays

A 3-(4,5-dimethylthiazol-2-yl)-2,5-diphenyltetrazolium bromide (MTT) cell proliferation assay and a LDH cytotoxicity assay were used to assess cell proliferation and death according to the manufacturer's instructions (American Type Culture Collection, Manassas, VA, and Pierce, respectively).

RESULTS

Intrapleural injection of LLC cells resulted in multiple discrete pleural tumors (8.6 ± 1.0 per animal) and a MPE (mean volume 667 ± 58 μl) by 14 d. Pleural carcinomatosis was lethal: Prolongation of the experimental duration resulted in 100% mortality by Day 17. When 1.5×10^5 LLC cells were injected, 100% of the animals yielded pleural effusions and pleural tumors ($n = 40$). In contrast, injection of 5×10^4 LLC cells resulted in incomplete penetrance (70% of mice had detectable pleural effusions, $n = 10$). To evaluate the presence of pleural effusions and pleural tumors in the living animal, we performed CT and FDG-PET scans on a subgroup of animals at Day 11. Free-floating bilateral pleural effusions and pleural tumor foci were clearly visible on CT scans. Overlays of CT and FDG-PET images of a control mouse and a mouse at 11 d after intrapleural tumor cell injection are shown in Figure 1. Tumor tissue showed increased radiotracer uptake on FDG-PET scanning in discrete areas in the thoracic cavity that corresponded to tumor foci and areas of pleural effusion formation (Figure 1, *right panel*).

At the time of harvest (14 d), pleural effusions could be directly visualized through the diaphragm, often surrounding tumor foci (Figure 2A). The pleural tumors were found to reside equally on the visceral and parietal pleura (Figure 2B). Histology confirmed that pleural tumors consisted of adenocarcinomatous cells growing on the pleural surfaces (Figure 2C). Larger pleural tumors formed bridges between the lung parenchyma and the thoracic cage and infiltrated neighboring anatomic structures, including lung, chest wall, mediastinum, and diaphragm (images not shown). Pleural tumors showed abundant new vessel formation (Figure 2D). No fibrous pleural adhesions were evident on gross examination.

Before analyzing the malignant pleural effusions, we evaluated the characteristics of pleural fluid in untreated C57B/6 mice ($n = 5$) (Table 1). The fluid was straw colored and slightly turbid. The mean recoverable volume was 16.2 × 1.4 μl, or ∼ 0.65 ± 0.05 ml/kg. The mean protein level was 1.07 ± 0.1 g/dl, and the mean glucose level was 167 ± 15 mg/dl. The cellular component consisted mainly of mesothelial cells, large lymphocytes, and macrophages (Figure 2E). The mean VEGF concentration was 88 ± 52 pg/ml.

A summary of the physical, cellular, and biochemical characters of the MPEs in this model in comparison to pleural fluid obtained from untreated mice is presented in Table 1. The pleural fluid appeared hemorrhagic but did not coagulate, and after centrifugation the supernatant was straw colored. By harvesting mice at serial time points (at 8, 10, and 12 d), we observed that MPEs formed gradually and that their red blood cell content increased stepwise (data not shown). Pleural fluid glucose levels and total protein levels in MPEs were similar to serum levels. LDH levels were elevated in comparison to matched serum values (Table 1). Differential cell counts in MPEs revealed a mixed inflammatory infiltrate interspersed with malignant cells (Figure 2F). The inflammatory cell population found in the pleural fluid consisted primarily of mononuclear cells, with lymphocytes, neutrophils, and eosinophils appearing in smaller numbers (Table 1). Mesothelial cells accounted for < 1% of cells in MPEs. Because mononuclear inflammatory cells were predominant in MPEs, we determined if this was associated with local production of monocyte chemoattractant chemokines. Indeed, pleural fluid levels of MCP-1 and MCP-5 were markedly elevated in MPEs (3,037 ± 31 pg/ml and 1,996 ± 204 pg/ml, respectively) compared with matched sera (136 ± 15 pg/ml and 74 ± 12 pg/ml, respectively).

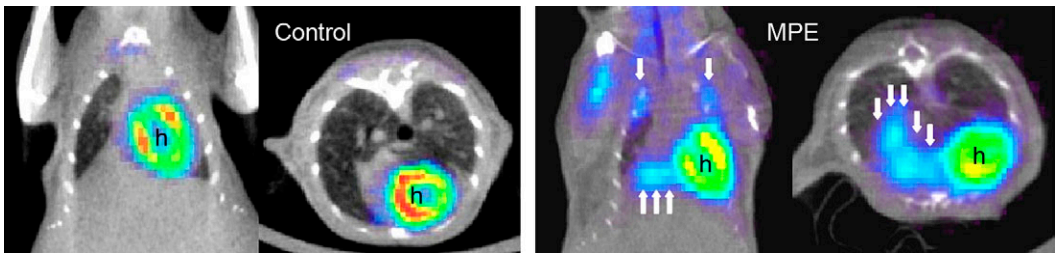

Figure 1. CT-PET imaging of developing pleural tumors and effusions. Coronal and transverse CT-PET co-registration images of an untreated mouse (*left panel*) and an animal that received intrapleural injection of 1.5×10^5 LLC cells at Day 11 after injection (*right panel*). Note the multiple intrathoracic sites of increased radiotracer uptake in the treated mouse that are absent in the normal mouse. These sites proved to be discrete pleural tumors at necropsy (*single arrows*) and areas of pleural fluid accumulation with associated tumor mass (*multiple arrows*). h = heart signal.

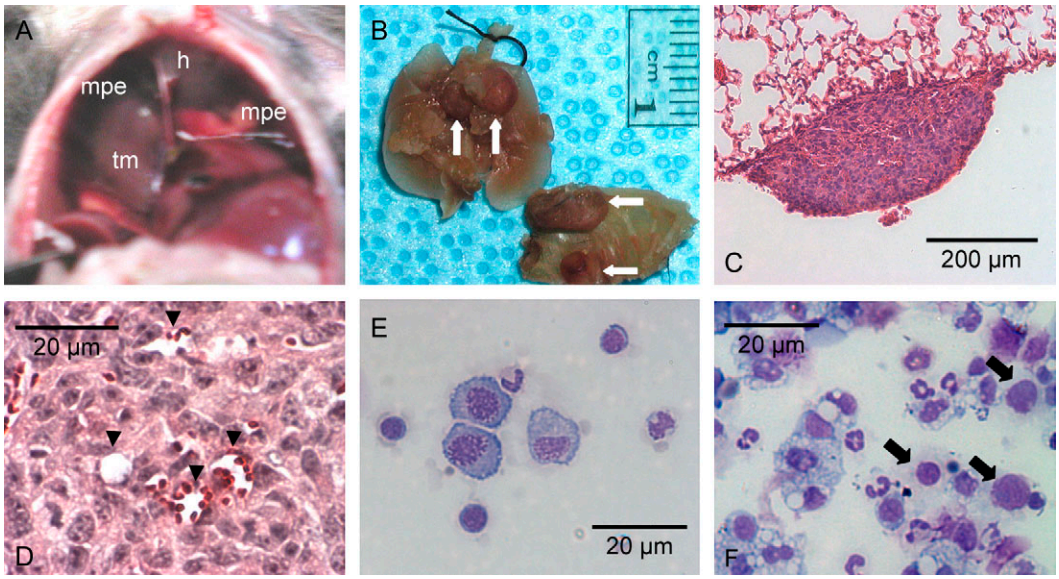

Figure 2. Malignant pleural effusions and pleural tumors in C57B/6 mice after intrapleural LLC propagation. (*A*) Transdiaphragmatic view of a malignant pleural effusion (mpe), a supradiaphragmatic tumor mass (tm), and the heart (h). (*B*) Lung and chest wall explants showing multiple tumor foci on the parietal and visceral pleura (*arrows*). (*C*) Section through a small visceral pleural Lewis lung cancer implantation stained with hematoxylin and eosin shows tumor growth on the pleural surface (Å = 100). (*D*) New vessel formation within a pleural LLC tumor (Å = 400, *arrowheads* = new vessels formed within tumor tissue). (*E*) Cytological preparation (cytospin) from pleural fluid obtained from an untreated mouse stained with modified Wright's-Giemsa stain (Å = 400). (*F*) Representative photomicrograph of a cytospin from a malignant pleural effusion stained with modified Wright's-Giemsa stain (Å = 400). LLC cells with large nuclei and visible nucleoli (*arrows*) can be observed among with a variety of host inflammatory cells.

The high protein and LDH content of MPEs compared with matched serum values were indicative of vascular hyperpermeability. In addition, VEGF levels in MPEs were increased 20- to 30-fold over matched sera and pleural fluid or serum from untreated mice (Table 1), implying local rather than systemic production of VEGF in the model. To determine whether MPEs in this model are characterized by increased vascular permeability, we measured leakage of Evans' blue dye into the pleural space. One hour after intravenous injection of 200 μl of 50 mg/ml Evans' blue solution (total dose 10 mg) in mice bearing MPEs (n = 8, Day 13), mean serum Evans' blue levels were 17.6 ± 3.2 μg/ml, and mean pleural effusion levels were 3.6 ± 0.9 μg/ml (26 ± 9% of serum levels). In untreated mice (n = 4), mean serum Evans' blue levels were 18.7 ± 4.1 μg/ml, and mean pleural fluid levels were 0.04 ± 0.02 μg/ml (< 1% of serum levels) (Table 1). In MPE, the presence of Evan's blue dye, which binds avidly to albumin, implies substantial protein extravasation into the pleural fluid.

To track NF-κB activation in LLC cells, we stably transfected cells with pNGL. In culture, pNGL LLC cells demonstrated high basal levels of NF-κB–dependent reporter expression as assessed by fluorescence microscopy or luciferase activity (data not shown). Basal NF-κB activity in LLC cells was not inhibited by confluent growth because bioluminescence emission was correlated with LLC cell number even at high cell densities *in vitro* (Figure 3A). GFP-expressing malignant cells in MPEs could be identified by fluorescence microscopy (Figure 3B). In addition, GFP-expressing cancer cells could be discriminated from wild-type LLC cells and from other pleural fluid cells and quantified using flow cytometry for GFP (Figures 3C and 3D). In MPEs, GFP+ cells comprised 45 ± 5% of total nucleated cells (Figure 3D). Less than 1% of GFP+ cells were also positive for the mouse myeloid lineage marker CD11b, confirming that GFP+ cells in the pleural fluid were tumor (pNGL LLC) cells (data not shown).

Stably transfected pNGL LLC cells exhibited NF-κB–driven reporter transgene expression during intrapleural propagation, facilitating intravital mapping of tumor cells by bioluminescent imaging (Figure 4A). Bioluminescence imaging was done to detect luciferase activity stemming from LLC cells after intravenous injection of 1 mg of D-luciferin. At early time points (up to Day 10), focal areas of bioluminescence emission were identified in the chest; however, at later time points (after Day 10), diffuse light emission was detectable over the entire thoracic cavity. At early time points, light emission coincided with the presence of discrete pleural tumors, whereas diffuse chest light emission was observed with gradual accumulation of substantial volumes of pleural fluid. The time-course of pleural tumor NF-κB activity as assessed by bioluminescent detection of luciferase activity was reproducible and approximated an ideal exponential curve (Figure 4B). Persistent NF-κB activity in LLC cells *in vivo* was confirmed by fluorescence microscopy revealing green fluorescence of pleural tumors in contrast to the adjacent anatomic structures (see Figure 3B). To determine whether NF-κB activity during pleural cancer progression was associated with expression of NF-κB–driven genes, we measured levels of TNF-α in the pleural fluid. We found a significant increase in TNF-α levels in MPEs compared with matched serum samples, whereas TNF-α was not detectable in pleural fluid or serum from untreated mice (Figure 4C).

In this model of MPE induced by intrapleural injection of pNGL LLC cells, we assessed the relationships between measures of tumor burden (pleural effusion volume and pleural surface tumor number) and integers of pleural tumor NF-κB activity (percentage of GFP+ cells in the pleural effusions and chest photon emission before animals were killed). The pleural surface tumor number correlated with pleural effusion volume (ρ = 0.618, P = 0.005) (Figure 5A). The percentage of GFP+ cells (malignant cells with active NF-κB) in the pleural fluid determined by flow cytometry correlated with pleural effusion volume (ρ = 0.624, P = 0.01) (Figure 5B) and pleural surface tumor number (ρ = 0.648, P = 0.007) (data not shown). Chest photon emission measured by bioluminescence imaging before animals were killed correlated with pleural effusion volume (ρ = 0.628, P = 0.004) (Figure 5C). These findings indicate that

TABLE 1. FEATURES OF MALIGNANT PLEURAL EFFUSIONS GENERATED IN C57B/6 MICE 14 d AFTER INTRAPLEURAL INJECTION OF 15 × 10^5 LLC CELLS (n = 9) COMPARED WITH UNTREATED MICE (n = 5).

Features	Untreated Mouse	Mouse MPE
Pleural fluid volume, μl	16.2 ± 1.4	667 ± 58
Pleural surface tumor number	0	8.6 ± 1.0
Red blood cells, $\times 10^3$/μl		
Pleural fluid	0	4.7 ± 0.55
Blood	8.2 ± 0.7	8.4 ± 0.15
Nucleated cells, $\times 10^3$/μl		
Pleural fluid	0.5 ± 0.2	32.7 ± 4.5
Blood	6.5 ± 1.3	8.0 ± 0.6
Pleural fluid tumor cells, $\times 10^3$/μl	0	14.7 ± 2.9
Pleural fluid cells, % of nontumor cells		
Mononuclear	72 ± 12	57 ± 5
Lymphocytes	22 ± 5	23 ± 6
Neutrophils	5 ± 3	13 ± 4
Eosinophils	1 ± 1	12 ± 2
Basophils	Occasional	Occasional
Glucose, mg/dl		
Pleural fluid	167 ± 15	208 ± 55
Serum	87 ± 5	214 ± 73
Protein, g/dl		
Pleural fluid	1.07 ± 0.1	2.18 ± 0.03
Serum	1.76 ± 0.31	1.67 ± 0.15
Ratio	0.6 ± 0.06	1.37 ± 0.14
LDH, U/l		
Pleural fluid	1,204 ± 105	6,850 ± 1,170
Serum	995 ± 204	1,213 ± 147
Ratio	1.21 ± 0.12	5.57 ± 0.62
VEGF, pg/ml		
Pleural fluid	88 ± 52	2,303 ± 284
Serum	64 ± 47	47 ± 29
Vascular hyperpermeability, pleural fluid/serum Evan's blue	No (< 1%)	Yes (26 ± 9%)

Definition of abbreviations: LDH, lactate dehydrogenase; LLC, Lewis lung cancer; MPE, malignant pleural effusion; VEGF, vascular endothelial growth factor.
Values represent mean ± SEM.

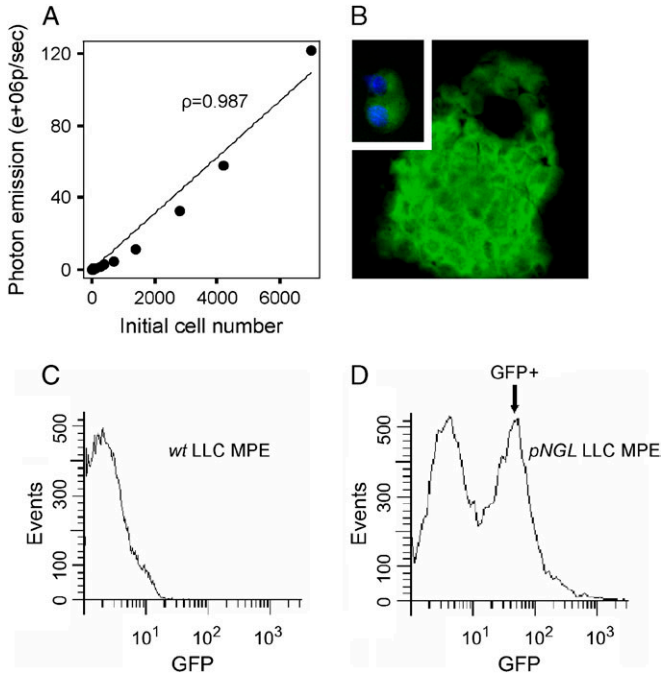

Figure 3. NF-κB is active in LLC cells. (*A*) NF-κB–driven luciferase expression by pNGL LLC cells plated in increasing numbers and imaged for bioluminescence after 3 d. The relationship between the initial cell number and subsequent bioluminescence emission is highly correlated (n = 12, ρ = 0.987, $P < 0.001$). (*B*) Fluorescent microscopic image of a cytological preparation (cytospin) from a malignant pleural effusion. Depicted is a clump of pNGL LLC cells with fluorescing cytoplasm and darker outlined nuclei. *Inlay*: Two isolated GFP+ LLC cells with nuclei counterstained with 4,6-diamidino-2-phenylindole (Å = 200 for both images). (*C*) Flow cytometric analysis of a malignant pleural effusion caused by wild-type LLC cells. A single peak of green fluorescence intensity is produced. (*D*) Flow cytometric analysis of malignant pleural fluid after intrapleural injection of pNGL (GFP-reporter–containing) LLC cells. GFP+ LLC cells are identified by increased fluorescence resulting in the formation of a discrete new peak (*arrow*).

in the MPE model, measures of tumor burden were associated with NF-κB activity in pleural tumors.

To assess the role of the NF-κB pathway in regulating tumor progression and effusion formation in the MPE model, we inhibited NF-κB activation in LLC cells by infection with a recombinant adenoviral vector expressing a dominant inhibitor (Ad-IκBα-DN) (21). Expression of IκBα-DN in pNGL LLC cells resulted in decreased NF-κB activity compared with cells infected with a control adenoviral vector as assessed by bioluminescent imaging (Figure 6A). These treatments did not affect LLC cell viability or proliferation in culture as assessed by trypan blue exclusion (data not shown), MTT cell proliferation assay (Figure 6B), and LDH cytotoxicity assay (Figure 6C) observed up to 120 h after infection. Despite sustained viability and proliferation, intrapleural injection of IκBα-DN–expressing LLC cells led to significant decreases in pleural effusion volume and pleural tumor formation at 14 d in comparison to LLC cells infected with a control adenoviral vector (Ad-βgal) (Figures 6D and 6E). The cellular and biochemical characters of MPEs generated by injection of Ad-IκBα-DN–infected cells did not differ significantly from MPEs generated by control virus-infected LLC cells (data not shown). TNF-α levels in MPEs generated by IκBα-DN–expressing LLC cells were significantly lower than in MPEs generated by LLC cells infected with a control adenoviral vector, suggesting that LLC cells are responsible for production of some NF-κB–dependent inflammatory mediators in this model (Figure 6F). VEGF, MCP-1, and MCP-5 levels were similar in MPEs induced by injection of IκBα-DN–expressing LLC cells or control LLC cells (data not shown). These findings indicate that NF-κB inhibition limits pleural effusion formation by a mechanism other than altered VEGF or MCP production.

DISCUSSION

In these studies, we have characterized a model of MPE in immunocompetent mice that is similar in many aspects to human MPE. Like human MPE, MPEs in this model are exudates with high protein and LDH content relative to matched serum (1). High levels of VEGF and monocyte chemoattractant chemokines, which seem to be produced locally in the pleural cavity in the mouse model of MPE, have been also found in MPEs in humans (22, 23). Tumor growth in the pleural cavity triggers a host immune response, evident by a mixed inflammatory cell component in pleural fluid that is similar to the inflammatory cells found in human MPE. High VEGF levels in MPEs, new vessel formation within tumors, and increased vascular permeability are mechanisms postulated to be involved in human MPE pathogenesis and are all present in this mouse model of MPE (1).

Using the pNGL LLC reporter cell line, we show that NF-κB is active in LLC cells during intrapleural propagation. In the

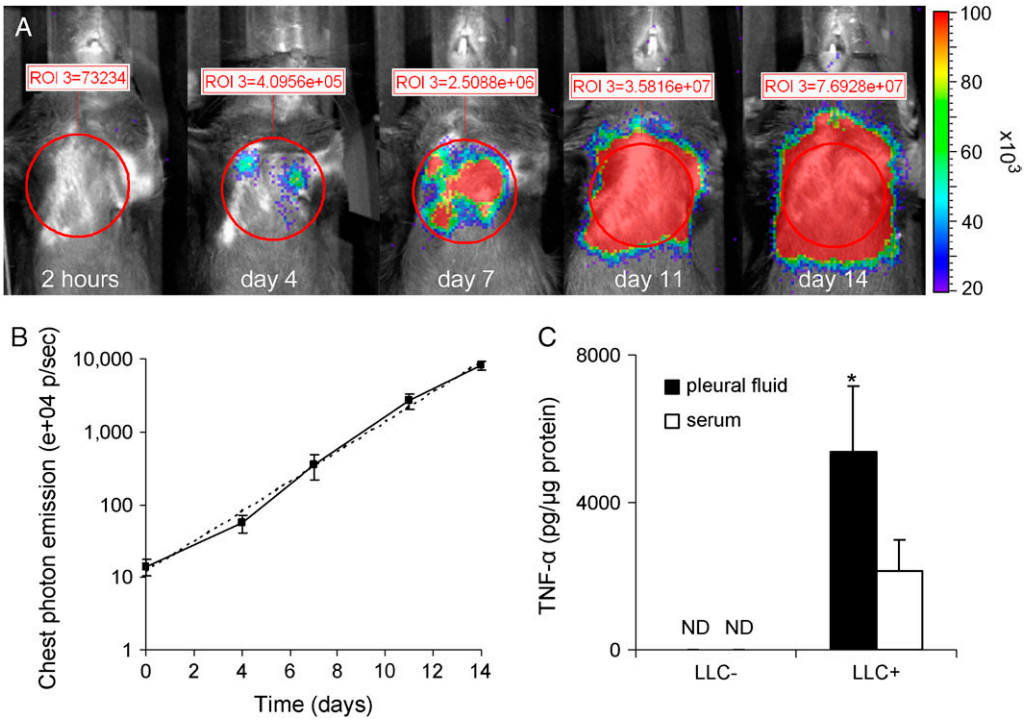

Figure 4. NF-κB activity in tumor cells during pleural cancer progression. (*A*) Time-course of bioluminescence emission after intrapleural propagation of 1.5×10^5 pNGL LLC cells in a representative C57B/6 mouse. The mouse was serially imaged after intravenous injection of luciferin (1 mg) at the time points indicated. Chest bioluminescence emission was measured by integration of photon flux within standard-sized regions of interest placed over the chest (*red circles*). The actual measurements are indicated in red numbers above the regions of interest. (*B*) Summary of bioluminescent imaging data acquired from nine mice as in (*A*) (logarithmic scale). The *dotted line* represents an ideal exponential curve. Every time point differs significantly from any other ($P < 0.01$). (*C*) TNF-α accumulation in MPEs. TNF-α levels were measured by ELISA in pleural fluid and serum obtained from LLC-treated and untreated mice ($n = 4$–8, $^*P = 0.03$ compared with sera from LLC-treated mice and $P < 0.001$ compared with samples from untreated mice). ND = not detectable.

presence of luciferin, light emission from these tumor cells serves as a tracer to map *in vivo* tumor growth, revealing that distinct pleural tumor implantations precede the appearance of effusions. The relationship between tumor mass and MPE volume is suggested by the correlation between number of pleural tumor foci and MPE volume. In this model of MPE, measures of pleural tumor NF-κB activity, including photon emission from the chest and numbers of GFP+ cells in the MPE, were correlated with measures of pleural tumor burden. Hence, tumor progression seemed to be associated with sustained pleural tumor NF-κB activity. In this regard, inhibition of NF-κB in LLC cells resulted in reduced pleural effusion volume and in a reduced number of tumor foci, providing additional evidence that the NF-κB pathway in tumor cells is tightly linked to tumor progression in this model.

An important advantage of our model compared with existing models of MPE is that in our model the host is immunocompetent. This is important for several reasons. First, the model

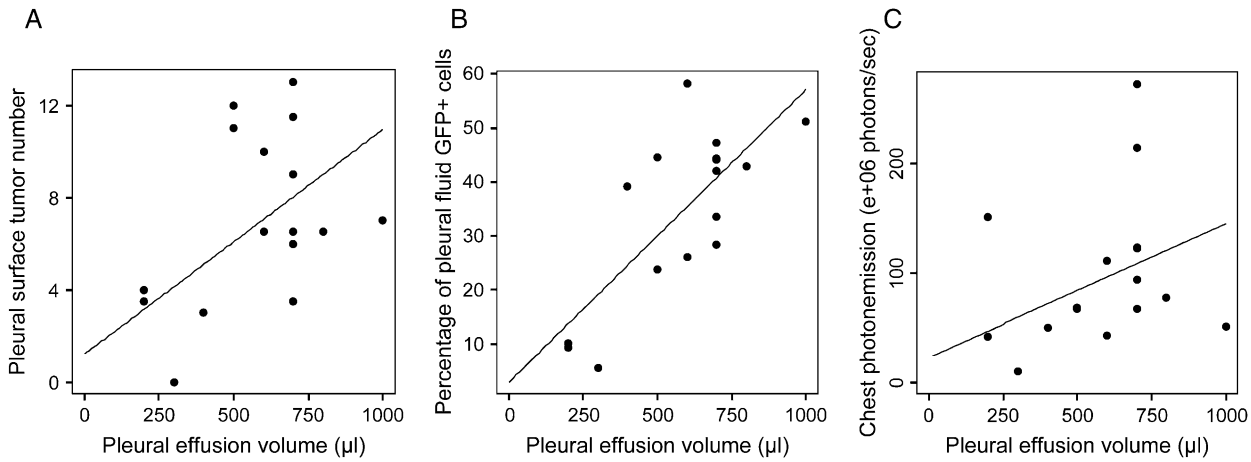

Figure 5. Indicators of tumor burden correlate with measurements of pleural tumor NF-κB activity. Shown are scatter plots and linear regression lines of pleural effusion volume compared with (*A*) pleural surface tumor number ($\rho = 0.618$, $P = 0.005$), (*B*) GFP+ (pNGL LLC) cells in the pleural fluid ($\rho = 0.624$, $P = 0.01$), and (*C*) chest photon emission measured by bioluminescent imaging on day of harvest ($\rho = 0.628$, $P = 0.004$). $n = 15$ for each graph.

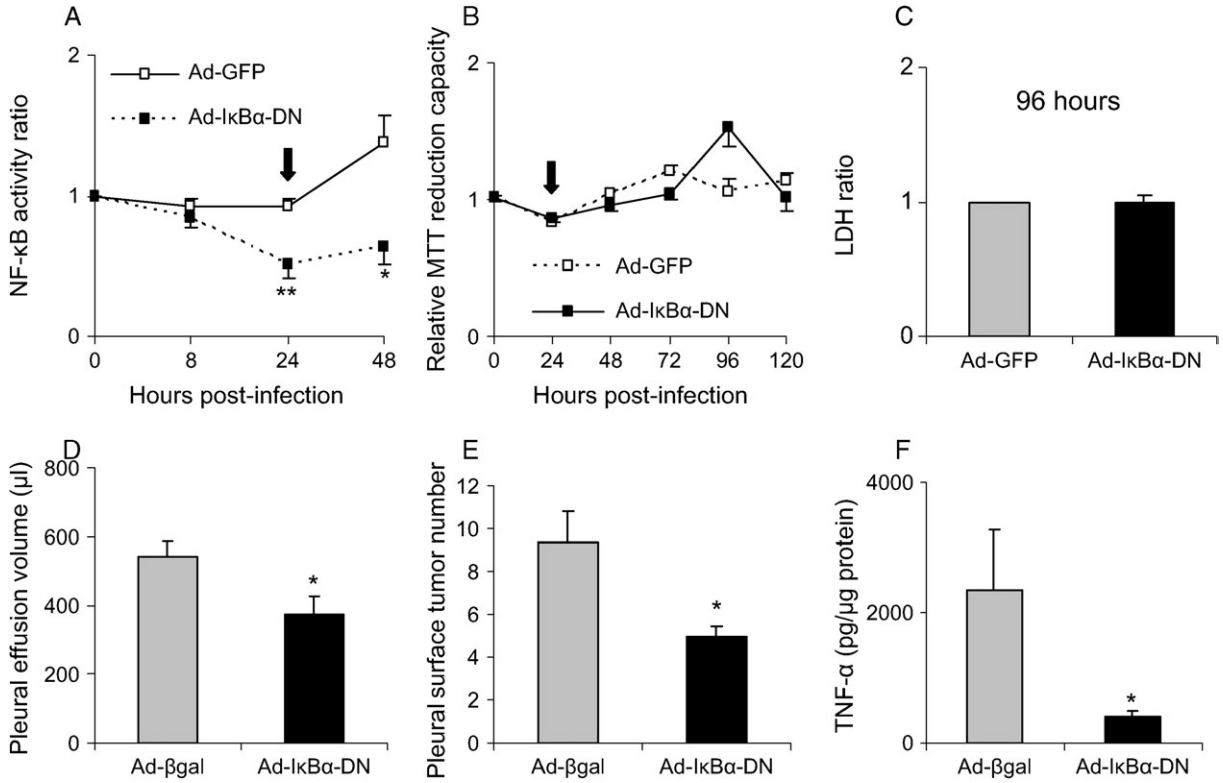

Figure 6. NF-κB regulates tumor progression in the MPE model. (*A*) Inhibition of the NF-κB pathway in LLC cells *in vitro* using a recombinant adenoviral vector encoding a dominant inhibitor (Ad-IκBα-DN). pNGL LLC cells were imaged for bioluminescence after infection with Ad-IκBα-DN or control adenovirus (Ad-GFP) at moi = 500 ($n = 3$ for each data point; $^*P < 0.05$, $^{**}P < 0.01$ compared with Ad-GFP). NF-κB activity of infected cells is shown after correction for NF-κB activity in control (uninfected) pNGL LLC cells in neighboring wells (NF-κB activity ratio). Data represent one of three experiments with similar findings. The *arrow* represents the timepoint selected for *in vivo* injection of cells after adenoviral infection. (*B*) Infection of LLC cells with Ad-IκBα-DN does not affect LLC cell proliferation. MTT reduction capacity was determined at several time points after infection with Ad-IκBα-DN or control adenovirus (Ad-GFP) at moi = 500 ($n = 3$ for each data point). The *arrow* represents the time point selected for *in vivo* injection of cells after adenoviral infection. (*C*) Infection of LLC cells with Ad-IκBα-DN does not increase cell death. LDH was measured in LLC cell culture supernatants and whole-cell lysates 96 h after cell infection as in (*A*). The supernatant/whole cell lysate LDH ratio is shown ($n = 4$ for each data point, $P = 0.56$). All *in vitro* experiments were done in triplicate. (*D*) NF-κB inhibition in LLC cells results in decreased pleural effusion accumulation. Mice were injected with LLC cells infected with Ad-IκBα-DN or Ad-βgal and harvested at 14 d ($n = 7$, $^*P = 0.031$). (*E*) NF-κB inhibition in LLC cells results in decreased numbers of pleural tumor foci compared with Ad-βgal control ($n = 7$, $^*P = 0.012$). (*F*) NF-κB inhibition in LLC cells results in lower pleural fluid TNF-α levels compared with Ad-βgal control ($n = 7$, $^*P = 0.042$).

closely resembles human MPEs, which are characterized by an influx of inflammatory cells (3). Second, the biological behavior of malignancies, including growth and metastasis, can be profoundly influenced by the development of a host immune response (24–28). Third, inflammatory and other host cells can produce mediators, including VEGF, that affect formation of pleural effusions (29–31). Therefore, the host immune response may be in part responsible for malignant pleural fluid accumulation. These issues are directly relevant for studies designed to investigate the pathogenesis and treatment of MPEs.

VEGF is a multi-potent molecule implicated in angiogenesis that may have an important role in MPE formation (32–34). This cytokine can be produced by various cell types, including many tumor cells and activated macrophages (29, 33). In addition to being a potent angiogenic factor, VEGF is a powerful inducer of vascular permeability (33, 35–38). Clinical studies have detected high levels of VEGF in human MPEs but not in corresponding sera, suggesting local production by tumor in the pleural cavity (22). Moreover, in a model of MPE in which human cancer cells were injected intravenously into immunodeficient mice, VEGF was shown to be a main effector of MPE formation (7). Although high levels of VEGF were identified in pleural fluid in our model, modulation of NF-κB activity reduced pleural effusion volume independent of VEGF levels, indicating that additional factors can regulate effusion formation in an immunocompetent host. NF-κB activity was evident in LLC cells during intrapleural tumor growth and can be used to visualize tumor progression in the MPE model. The NF-κB pathway is a key regulator of proinflammatory gene transcription in many cell types, including cancer cells, and can affect tumor progression by influencing cell survival, tissue remodeling, and angiogenesis (10, 11, 39–41). Our data indicate that NF-κB activity promotes intrapleural accumulation of the proinflammatory cytokine TNF-α; however, the specific NF-κB–dependent factors that regulate MPE formation in this model are yet to be determined.

Bioluminescence imaging technology is applied to trace molecules and cells *in vivo* or to assess gene-specific transcriptional activity in cell-culture systems or in living animals (42, 43). In these studies, we took advantage of basal NF-κB activity in cancer cells to drive luciferase expression. Bioluminescent images could accurately predict the presence of pleural tumors, as confirmed by necropsy and histology, and allowed serial visualization of pleural carcinomatosis in the same animals. Thus, our

reporter facilitated intravital mapping of tumor tissue in the living host.

MPE is a common problem for cancer patients, especially those suffering from lung cancer. Its treatment is not ideal, and novel therapeutic strategies are desperately needed. Because the pathogenesis of MPE is not adequately understood, further research is necessary regarding tumor–host interactions in cancerous involvement of the pleura. This MPE model provides some important advantages for future investigations. By providing reproducible end-points after predetermined latency, this model is a powerful tool to investigate the mechanisms and treatment of MPE. Using this model, we identified the NF-κB pathway as one potential therapeutic target in MPE.

Conflict of Interest Statement: None of the authors has a financial relationship with a commercial entity that has an interest in the subject of this manuscript.

Acknowledgments: The authors thank Janet F. Shelton for professional editorial assistance and Robyn A. Elkin for animal care assistance.

References

1. Light RW. Pleural diseases, 4th ed. Philadelphia: Lippincott, Williams and Wilkins; 2001.
2. Antony VB, Loddenkemper R, Astoul P, Boutin C, Goldstraw P, Hott J, Panadero FR, Sahn SA. Management of malignant pleural effusions. *Am J Respir Crit Care Med* 2000;162:1987–2001.
3. Sahn SA. Malignant pleural effusions. In: Fishman AP, Elias JA, Fishman JA, Grippi MA, Kaiser LR, Senior RM, editors. Fishman's pulmonary diseases and disorders, 3rd ed. New York: McGraw-Hill; 1998. pp. 1429–1438.
4. Sugiura S, Ando Y, Minami H, Ando M, Sakai S, Shimokata K. Prognostic value of pleural effusion in patients with non-small cell lung cancer. *Clin Cancer Res* 1997;3:47–50.
5. Naito T, Satoh H, Ishikawa H, Yamashita YT, Kamma H, Takahashi H, Ohtsuka M, Hasegawa S. Pleural effusion as a significant prognostic factor in non-small cell lung cancer. *Anticancer Res* 1997;17:4743–4746.
6. Light RW. Talc for pleurodesis? *Chest* 2002;122:1506–1508.
7. Yano S, Shinohara H, Herbst RS, Kuniyasu H, Bucana CD, Ellis LM, Fidler IJ. Production of experimental malignant pleural effusions is dependent on invasion of the pleura and expression of Vascular Endothelial Growth Factor/Vascular Permeability Factor by human lung cancer cells. *Am J Pathol* 2000;157:1893–1903.
8. Yano S, Nokihara H, Hanibuchi M, Parajuli P, Shinohara T, Kawano T, Sone S. Model of malignant pleural effusion of human lung adenocarcinoma in SCID mice. *Oncol Res* 1997;9:573–579.
9. Yano S, Herbst RS, Shinohara H, Knighton B, Bucana CD, Killion JJ, Wood J, Fidler IJ. Treatment for malignant pleural effusion of human lung adenocarcinoma by inhibition of vascular endothelial growth factor receptor tyrosine kinase phosphorylation. *Clin Cancer Res* 2000; 6:957–965.
10. Dong G, Chen Z, Kato T, Van Waes C. The host environment promotes the constitutive activation of nuclear factor-κB and proinflammatory cytokine expression during metastatic tumor progression of murine squamous cell carcinoma. *Cancer Res* 1999;59:3495–3504.
11. Bharti AC, Aggarwal BB. Nuclear factor-kappa B and cancer: its role in prevention and therapy. *Biochem Pharmacol* 2002;64:883–888.
12. Milligan SA, Nopajaroonsri C. Inhibition of NF-κB with proteasome inhibitors enhances apoptosis in human lung adenocarcinoma cells in vitro. *Anticancer Res* 2001;21:39–44.
13. Jones DR, Broad RM, Madrid LV, Baldwin AS Jr, Mayo MW. Inhibition of NF-κB sensitizes non-small cell lung cancer cells to chemotherapy-induced apoptosis. *Ann Thorac Surg* 2000;70:930–936.
14. Batra RK, Guttridge DC, Brenner DA, Dubinett SM, Baldwin AS, Boucher RC. IκBα gene transfer is cytotoxic to squamous-cell lung cancer cells and sensitizes them to tumor necrosis factor-α mediated death. *Am J Respir Cell Mol Biol* 1999;21:238–245.
15. Mukhopadhyay T, Roth JA, Maxwell SA. Altered expression of the p50 subunit of the NF-κB transcription factor complex in non-small cell lung carcinoma. *Oncogene* 1995;11:999–1003.
16. Chen H-H, Fukumoto S, Furukawa K, Nakao A, Akiyama S, Urano T, Furukawa K. Suppression of lung metastasis of mouse Lewis lung cancer P29 with transfection of the ganglioside GM2/GD2 synthase gene. *Int J Cancer* 2003;103:169–176.
17. Takenaga K, Nakamura Y, Sakiyama S. Expression of antisense RNA to S100A4 gene encoding an S100-related calcium-binding protein suppresses metastatic potential of high-metastatic Lewis lung carcinoma cells. *Oncogene* 1997;14:331–337.
18. Harmey JH, Bucana C, Lu W, Byrne AM, McDonnell S, Lynch C, Bouchier-Hayes D, Dong Z. Lipopolysaccharide-induced metastatic growth is associated with increased angiogenesis, vascular permeability and tumor cell invasion. *Int J Cancer* 2002;101:415–422.
19. Sadikot RT, Jansen ED, Blackwell TR, Zoia O, Yull F, Christman JW, Blackwell TS. High-dose dexamethasone accentuates nuclear factor-κB activation in endotoxin-treated mice. *Am J Respir Crit Care Med* 2001;164:873–878.
20. Sadikot RT, Debelak JP, Jansen DE, Debelak JP, Yull FE, Christman JW, Blackwell TS, Chapman WC. Hepatic cryoablation-induced multisystem injury: bioluminescent detection of NF-κB activation in a transgenic mouse model. *J Gastrointest Surg* 2002;6:264–270.
21. Sadikot RT, Han W, Everhart MB, Zoia O, Peebles RS, Jansen ED, Yull FE, Christman JW, Blackwell TS. Selective IκB Kinase expression in airway epithelium generates neutrophilic lung inflammation. *J Immunol* 2003;170:1091–1098.
22. Kraft A, Weindel K, Ochs A, Marth C, Zmija J, Schumacher P, Unger C, Marme D, Gastl G. Vascular endothelial growth factor in the sera and effusions of patients with malignant and nonmalignant disease. *Cancer* 1999;85:178–187.
23. Antony VB, Godbey SW, Kunkel SL, Hott JW, Hartman DL, Burdick MD, Strieter RM. Recruitment of inflammatory cells to the pleural space: chemotactic cytokines, IL-8, and monocyte chemotactic peptide-1 in human pleural fluids. *J Immunol* 1993;151:7216–7223.
24. Frisch M, Biggar RJ, Engels EA, Goedert JJ. AIDS-Cancer Match Registry Study Group. Association of cancer with AIDS-related immunosuppression in adults. *JAMA* 2001;285:1736–1745.
25. Gallagher B, Zhengyan W, Schymura M, Kahn A, Fordyce EJ. Cancer incidence in New York State acquired immunodeficiency syndrome patients. *Am J Epidemiol* 2001;154:544–556.
26. Chiao EY, Krown SE. Update on non-acquired immunodeficiency syndrome-defining malignancies. *Curr Opin Oncol* 2003;15:389–397.
27. Sugiyama Y, Kato M, Chen F-A, Williams SS, Kawaguchi Y, Miya K, Jong YS, Mathiowitz E, Egilmez NK, Bankert RB. Human inflammatory cells within the tumor microenvironment of lung tumor xenografts mediate tumor growth suppression in situ that depends on and is augmented by Interleukin-12. *J Immunother* 2001;24:37–45.
28. Batra RK, Lin Y, Sharma S, Dohadwala M, Luo J, Pold M, Dubinett SM. Non-small cell lung cancer-derived soluble mediators enhance apoptosis in activated T lymphocytes through an IκB Kinase-dependent mechanism. *Cancer Res* 2003;63:642–646.
29. Kiriakidis S, Andreakos E, Monaco C, Foxwell B, Feldmann M, Paleolog E. VEGF expression in human macrophages is NF-κB-dependent: studies using adenoviruses expressing the endogenous NF-kB inhibitor IκBa and a kinase-defective form of the IκB kinase 2. *J Cell Sci* 2003; 116:665–674.
30. Yoshida S, Ono M, Shono T, Izumi H, Ishibashi T, Suzuki H, Kuwano M. Involvement of interleukin-8, vascular endothelial growth factor, and basic fibroblast growth factor in tumor necrosis factor alpha-dependent angiogenesis. *Mol Cell Biol* 1997;17:4015–4023.
31. Distler JHW, Hagen C, Hirth A, Mueller-Ladner U, Lorenz HM, del Rosso A, Michel BA, Gay RE, Nanagara N, Nishioka K, *et al.* Bucillamine induces the synthesis of vascular endothelial growth factor dose-dependently in systemic sclerosis fibroblasts via nuclear factor-κB and simian virus 40 promoter factor 1 pathways. *Mol Pharmacol* 2004; 65:389–399.
32. Ferrara N, Carver-Moore K, Chen H, Dowd M, Lu L, O'Shea KS, Powell-Braxton L, Hillan KJ, Moore MW. Heterozygous embryonic lethality induced by targeted inactivation of the VEGF gene. *Nature* 1996;380: 439–442.
33. Ferrara N. The role of vascular endothelial growth factor in the regulation of blood vessel growth. In: Bicknell R, Lewis CE, Ferrara N, editors. Tumor angiogenesis. New York: Oxford University Press; 1997. pp. 185–199.
34. Carmeliet P, Ferreira V, Breier G, Pollefeyt S, Kieckens L, Gertsenstein M, Fahrig M, Vandenhoeck A, Harpal K, Eberhardt C, *et al.* Abnormal blood vessel development and lethality in embryos lacking a single VEGF allele. *Nature* 1996;380:435–439.
35. Ferrara N, Henzel WJ. Pituitary follicular cells secrete a novel heparin-binding growth factor specific for vascular endothelial cells. *Biochem Biophys Res Commun* 1989;161:851–859.
36. Pepper MS, Ferrara N, Orci L, Montesana R. Vascular endothelial growth factor (VEGF) induces plasminogen activators and plasminogen

activator inhibitor type 1 in microvascular endothelial cells. *Biochem Biophys Res Commun* 1991;181:902–908.
37. Unemori E, Ferrara N, Bauer EA, Amento EP. Vascular endothelial growth factor induces interstitial collagenase expression in human endothelial cells. *J Cell Physiol* 1992;153:557–562.
38. Kumar R, Yoneda J, Bucana CD, Fidler IJ. Regulation of distinct steps of angiogenesis by different angiogenic molecules. *Int J Oncol* 1998; 12:749–757.
39. Blackwell TS, Christman JW. The role of nuclear factor-κB in cytokine gene regulation. *Am J Respir Cell Mol Biol* 1997;17:3–9.
40. Huang S, Pettaway CA, Uehara H, Bucana CD, Fidler IJ. Blockade of NF-κB activity in human prostate cancer cells is associated with suppression of angiogenesis, invasion, and metastasis. *Oncogene* 2001; 20:4188–4197.
41. Huang S, Robinson JB, DeGuzman A, Bucana CD, Fidler IJ. Blockade of nuclear factor-κB signaling inhibits angiogenesis and tumorigenicity of human ovarian cancer cells by suppressing expression of vascular endothelial growth factor and interleukin 8. *Cancer Res* 2000;60:5334–5339.
42. Weissleder R. Scaling down imaging: molecular mapping of cancer in mice. *Nat Rev Cancer* 2002;2:1–8.
43. Contag CH, Bachmann MH. Advances in in vivo bioluminescence imaging of gene expression. *Annu Rev Biomed Eng* 2002;4:235–260.